Publishing House
AKAPIT

COMPUTER METHODS IN MATERIALS SCIENCE
Informatyka w Technologii Materiałów

Vol. 7, 2007, No. 2

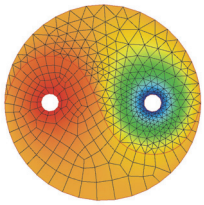

DISCRETE ELEMENT MODELLING OF ROCK CUTTING

JERZY ROJEK

Institute of Fundamental Technological Research
Swietokrzyska 21, 00-049 Warszawa, Poland

Abstract

The present paper presents modelling of rock cutting processes using the discrete element method. Numerical algorithm of the discrete element method employing cylindrical and spherical elements has been implemented and numerical simulation of rock cutting has been carried out. Numerical values of cutting forces have been compared with the theoretical values obtained from analytical formulae.

Key words: rock cutting, discrete element method, numerical simulation

1. INTRODUCTION

Mechanical rock cutting is a process encountered in different engineering works in rock excavation in mining industry or civil engineering. It is the main action performed by mining and tunneling machines like rock cutters, roadheaders, tunnel boring machines, drilling and boring machines, trenchers and dredges. Simulation of rock cutting could be very useful in the design of rock cutting tools and rock cutting processes. Numerical methods based on the continuum models have serious problems in modelling discontinuities of the material occuring during rock cutting Podgórski and Jonak (2004). Present paper presents possibilities of modelling rock cutting using discrete element model Rojek et al. (2001); Huang (1999).

2. PHYSICAL PHENOMENA IN ROCK CUTTING

Rock fracturing and fragmentation are the main physical phenomena during rock fracturing and fragmentation rock cutting. The type of failure during rock cutting depends on the type of rock, basically we can distinguish brittle and ductile failure. Figure 1 shows laboratory test of rock cutting with typical brittle failure which is characterized by chip formation and separation due to combined action of shear and tensile fracture initiated in a crushing zone near the tooth tip and propagating into the intact rock.

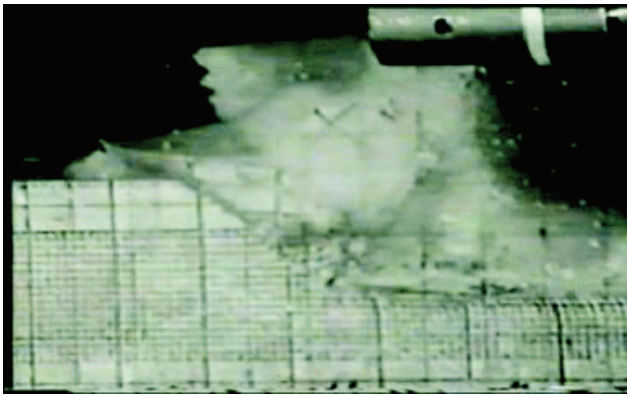

Fig. 1. *Laboratory test of rock cutting.*

3. ANALYTICAL MODELS OF ROCK CUTTING

Simple analytical models have been created in attempt to describe cutting processes, particularly

ISSN 1641-8581

those with brittle failure. One of the earliest models is that developed by Evans (1965) for rock cutting with drag picks. It is assumed that the breakage is essentially tensile and occurs along failure surface, which approximates a circular arc (figure 2a). The following formula for the cutting force is derived:

$$F_c = \frac{2\sigma_t dw \sin ½(90-\alpha)}{1-\sin ½(90-\alpha)}, \qquad (1)$$

where σ_t is tensile strength, d is depth of cut, w is width of the tool and α is the rake angle.

Engng, 6(4), 279–304.

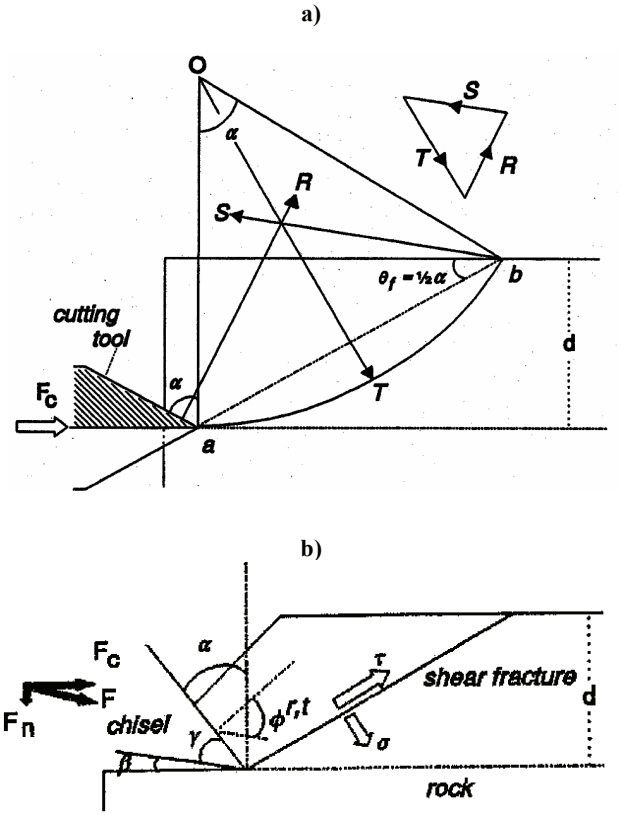

Fig. 2. Analytical models of rock cutting: a) Evans' model, b) Nishimatsu's model.

Another two-dimensional model is that developed by Nishimatsu (1972) who assumed that failure is purely due to shear and occurs along a plane (figure 2b). The following equation for resulting force F is obtained:

$$F = \frac{2\tau_u dw \cos\phi}{(n+1)(1-\sin(\phi^{r,t}+\phi-\alpha))}, \qquad (2)$$

where τ_u is the unconfined shear strength, d is depth of cut, w is width of the tool, $\phi^{r,t}$ is the angle of sliding friction rock-tool, ϕ is the angle of internal friction of intact rock, α is the rake angle, and n is the stress distribution factor obtained from the tests.

4. BASIC ASSUMPTIONS OF THE NUMERICAL MODEL

A numerical model of the tool-rock system allowing us to simulate a process of rock cutting is developed within the framework of the spherical discrete element method (DEM). This method is widely recognized as a suitable tool to model geomaterials with discontinuities Cundall and Strack (1979); Williams and O'Connor (1999); Rojek et al. (2001). The main physical phenomenon considered is the interaction of the tool with a rock leading to failure of the rock characterized with discontinuous material behaviour. Rock material will be modelled using the discrete element method. The tool is considered rigid in our numerical model assuming that its stiffness is sufficient to produce rock failure and its deformation is irrelevant for the purposes of modelling of rock failure.

5. DISCRETE ELEMENT METHOD FORMULATION

Within the DEM, it is assumed that a solid material can be represented as a collection of rigid particles/blocks interacting among themselves in the normal and tangential directions. Particles/blocks can be of arbitrary shape, here, the spherical (in 3D) and cylindrical (in 2D) particles are employed. Discrete element formulation using spherical or cylindrical particles was first proposed by Cundall and Strack (1979); Cundall (1988). Similar formulation has been developed by Rojek et al. (2001) and implemented in the explicit dynamic finite element code Simpact.

The translational and rotational motion of rigid spherical or cylindrical elements (particles) is governed by the standard equations of rigid body dynamics. For the i-th element we have

$$m_i \ddot{\mathbf{u}}_i = \mathbf{F}_i, \qquad I_i \dot{\boldsymbol{\omega}}_i = \mathbf{T}_i, \qquad (3)$$

where $\mathbf{u}$ is the element centroid displacement in a fixed (inertial) coordinate frame $\mathbf{X}$, $\boldsymbol{\omega}$ – the angular velocity, m – the element mass, I – the moment of inertia, $\mathbf{F}$ – the resultant force, and $\mathbf{T}$ – the resultant moment about the central axes. Vectors $\mathbf{F}$ and $\mathbf{T}$ are sums of all forces and moments applied to the i-th element due to external load, contact interactions with neighbouring spheres and other obstacles, as well as forces resulting from damping in the system. The form of the rotational equation (3) is valid for spheres and cylinders (in 2D) and is simplified with respect to a general form for an arbitrary rigid body.

Equations of motion (3) are integrated in time using a central difference scheme. The time integration operator for the translational motion at the *n*-th time step is as follows:

$$\ddot{\mathbf{u}}_i^n = \frac{\mathbf{F}_i^n}{m_i}, \tag{4}$$

$$\dot{\mathbf{u}}_i^{n+1/2} = \dot{\mathbf{u}}_i^{n-1/2} + \ddot{\mathbf{u}}_i^n \Delta t, \tag{5}$$

$$\mathbf{u}_i^{n+1} = \mathbf{u}_i^n + \dot{\mathbf{u}}_i^{n+1/2} \Delta t. \tag{6}$$

The first two steps in the integration scheme for the rotational motion are identical to those given by equations (4) and (5):

$$\dot{\boldsymbol{\omega}}_i^n = \frac{\mathbf{T}_i^n}{I_i}, \tag{7}$$

$$\boldsymbol{\omega}_i^{n+1/2} = \boldsymbol{\omega}_i^{n-1/2} + \dot{\boldsymbol{\omega}}_i^n \Delta t, \tag{8}$$

The vector of incremental rotation $\Delta\boldsymbol{\theta} = \{\Delta\theta_x \; \Delta\theta_y \; \Delta\theta_z\}^T$ is calculated as

$$\Delta\boldsymbol{\theta}_i = \boldsymbol{\omega}_i^{n+1/2} \Delta t, \tag{9}$$

If necessary it is also possible to track the total change of rotational position of particles. Explicit integration in time yields high computational efficiency of the solution for a single step. The disadvantage of the explicit integration scheme is its conditional numerical stability imposing the limitation on the time step Δt. The time step Δt must not be larger than a critical time step Δt_{cr}

$$\Delta t \le \Delta t_{\text{cr}} \tag{10}$$

determined by the highest natural frequency of the system $\omega_{\max}$

$$\Delta t_{\text{cr}} = \frac{2}{\omega_{\max}}. \tag{11}$$

Exact determination of the highest frequency $\omega_{\max}$ would require solution of the eigenvalue problem defined for the whole system of connected rigid particles. In an approximate solution procedure adopted, the maximum frequency is estimated as the maximum of natural frequencies of mass–spring systems defined for the contact pairs of particles.

The contact force between two particles **F** can be deomposed into normal and tangential components, $\mathbf{F}_n$ and $\mathbf{F}_T$, respectively

$$\mathbf{F} = \mathbf{F}_n + \mathbf{F}_T = \mathbf{n}F_n + \mathbf{F}_T, \tag{12}$$

where **n** is the unit vector normal to the particle surface at the contact point.

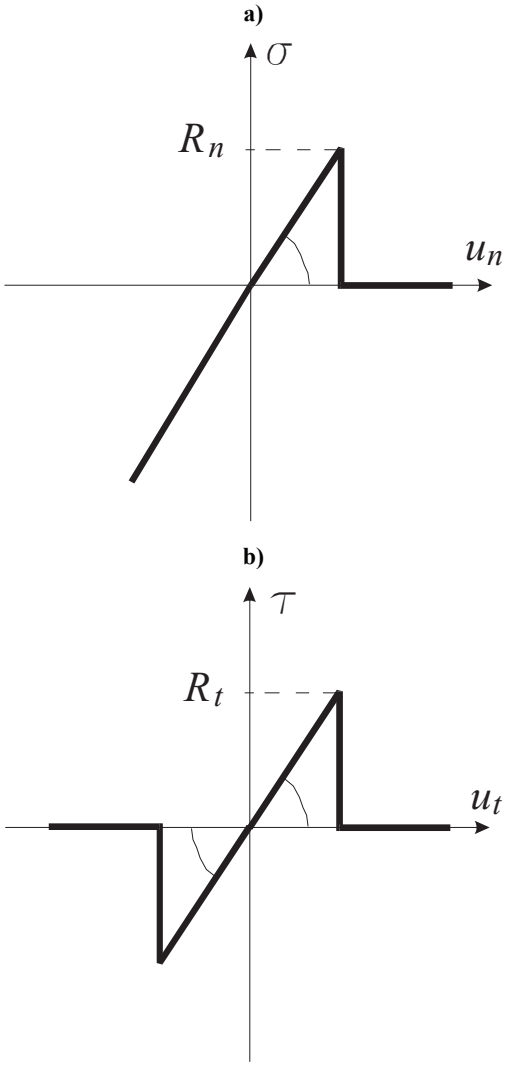

Fig. 3. *Force–displacement relationships for the elastic perfectly brittle model: a) in the normal direction, b) in the tangential direction.*

The contact forces F_n and $\mathbf{F}_T$ are obtained using a constitutive model formulated for the contact between two rigid spheres. In the present formulation rock materials are modelled using elastic perfectly brittle model of contact interaction, where we assume initial bonding for the neighbouring particles. These bonds can be broken under load allowing us to simulate initiation and propagation of material fracture. Contact laws for the normal and tangential direction for the elastic perfectly brittle model are shown in figure 3. When two particles are bonded the contact forces in both normal and tangential directions are calculated from the linear constitutive relationships:

$$F_n = k_n u_n , \qquad \|\mathbf{F}_T\| = k_t \|\mathbf{u}_t\|, \tag{13}$$

where: k_n – interface stiffness in the normal direction, k_t – interface stiffness in the tangential direction, u_n – normal relative displacement, $\mathbf{u}_t$ – tangential relative displacement.

The tensile and shear contact forces are limited by the tensile and shear interface strengths, R_n and R_t, respectively:

$$\sigma \le R_n , \qquad \|\boldsymbol{\tau}\| \le R_t . \tag{14}$$

Cohesive bonds are broken instantaneously when the interface strength is exceeded either by the tangential contact force or by the tensile contact force.

In the absence of cohesion the normal contact force can be compressive only ($\sigma \le 0$) and tangential contact force can be nonzero due to friction. In the present formulation the Coulomb model of friction is used.

A quasi-static state of equilibrium of the assembly of particles can be achieved by application of adequate damping. Damping is necessary to dissipate kinetic energy. Damping terms $\mathbf{F}_i^{\text{damp}}$ and $\mathbf{T}_i^{\text{damp}}$ are added to equations of motion (3)

$$m_i \ddot{\mathbf{u}}_i = \mathbf{F}_i + \mathbf{F}_i^{\text{damp}} , \quad I_i \dot{\boldsymbol{\omega}}_i = \mathbf{T}_i + \mathbf{T}_i^{\text{damp}} . \tag{15}$$

Damping implemented used in the present work is of non-viscous type and is given by:

$$\mathbf{F}_i^{\text{damp}} = -\alpha^t \|\mathbf{F}_i\| \frac{\dot{\mathbf{u}}_i}{\|\dot{\mathbf{u}}_i\|}, \; \mathbf{T}_i^{\text{damp}} = -\alpha^r \|\mathbf{T}_i\| \frac{\boldsymbol{\omega}_i}{\|\boldsymbol{\omega}_i\|} , \tag{16}$$

where α^t and α^r, are respective damping constants for translational and rotational motion.

6. STUDY OF MECHANICAL MATERIAL PROPERTIES

A study of material properties is the first step in our simulation of rock cutting process. A set of micromechanical parameters has to be established to model required macroscopic properties of the rock material which will be considered in the wear simulation. Macroscopic material properties are determined by laboratory tests such as unconfined compression test or indirect tension (Brazilian) test. The most important macroscopic properties are Young modulus E, Poisson ratio ν and compressive and tensile strengths, σ_c and σ_t, respectively. Microscopic parameters are, in turn, all the constitutive model parameters governing the interaction between a pair of particles: the normal and tangential stiffness k_n and k_T, the interface strengths in the normal and tangential directions, R_n and R_T, respectively, the Coulomb friction coefficient μ, and the contact damping coefficient α.

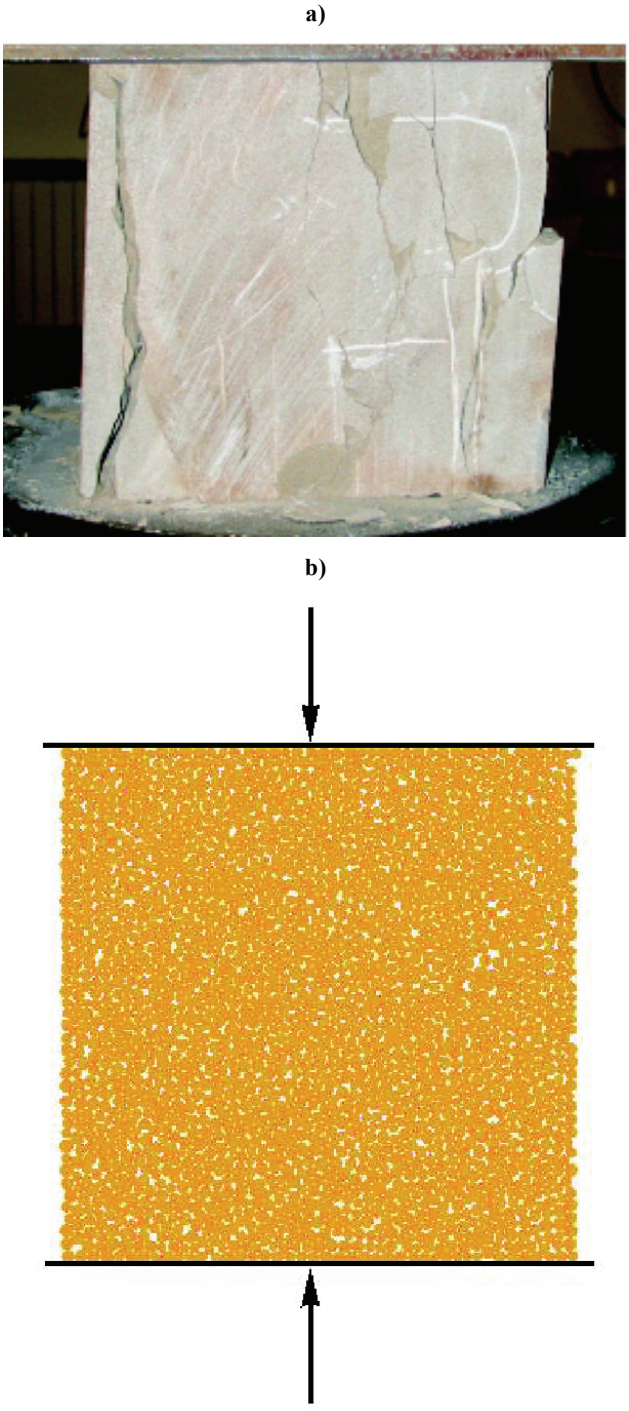

Fig. 4. Unconfined compression test: a) rock specimen after test, b) set-up of the numerical model.

The parameters of numerical discrete element model can be obtained carrying out simulations of laboratory tests combined with the systematic in-

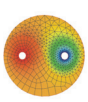

verse analysis, in our tests, however, we have used a simple trial-and-error approach.

We shall consider the sandstone with the following the Young modulus E = 14 GPa, unconfined compressive strength σ_c = 60 MPa, and tensile strength of σ_t = 10 MPa. Figure 4 shows a cube specimen of the rock after unconfined compression test.

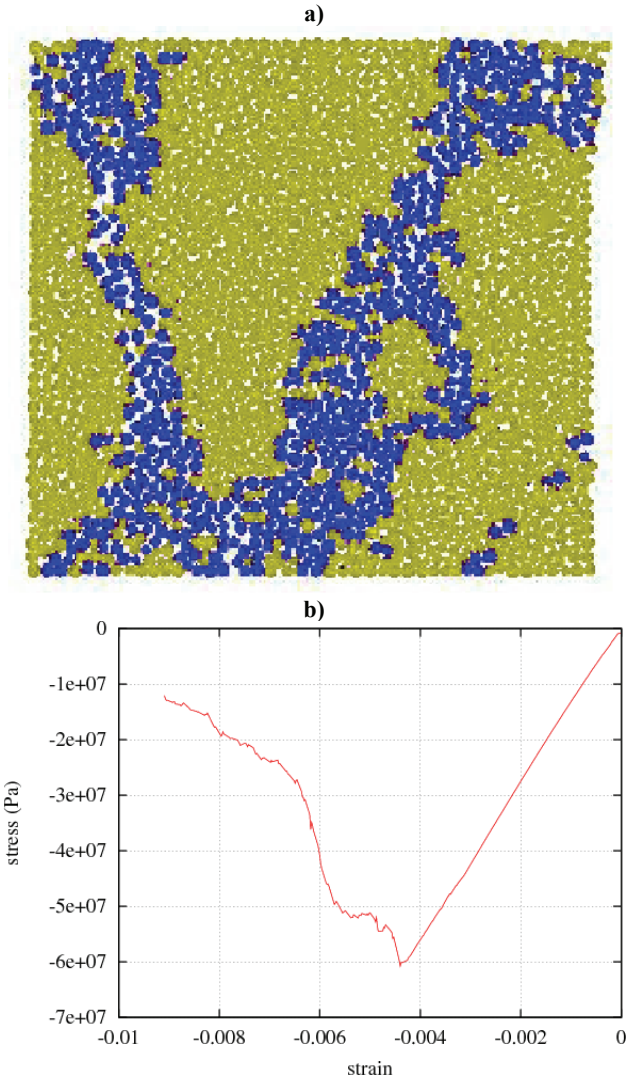

Fig. 5. *Simulation of unconfined compression test: a) failure mode (particles with broken cohesive bonds are marked with different colour), b) stress–strain relationship.*

The macroscopic response of a square material sample subjected to uniaxial compression has been studied numerically in order to determine the microscopic parameters of the discrete element model. Figure 4b presents the material sample prepared for testing. A material sample of 109×109 mm is represented by an assembly of randomly compacted 2100 discs of radii 1–1.5 mm. The loading has been introduced prescribing the motion of rigid plates pressing on the top and bottom of the sample with velocity 1 mm/s.

The following set of of micromechanical parameters has been found: $k_n = k_T$ = 20 GPa, μ = 0.839, R_n = 0.1 MN/m and R_T = 1 MN/m, $\alpha^t = \alpha^r$ t = 0.2. The results obtained using these parameters are shown in figure 5. The failure mode of the rock specimen is shown in figure 5a, and the stress-strain relationship shown in figure 5b.

Tensile strength of rocks is usually obtained experimentally from indirect tension (Brasilian) test. In the numerical procedure, however, we checked the tensile strength of the rock specimen model carrying out simulations of direct tension test. Failure mode is shown in figure 6a and stress–strain relationship obtained is plotted in figure 6b. The tensile strength obtained is σ_t = 12.7 MPa.

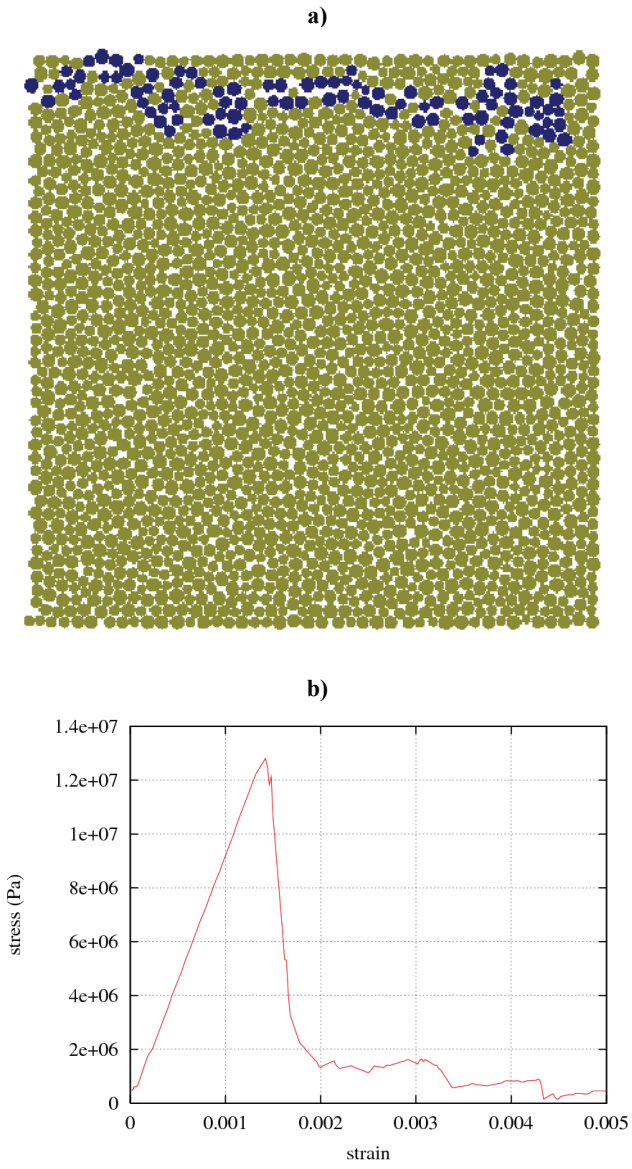

Fig. 6. *Simulation of uniaxial direct tension test: b) failure mode, b) stress–strain relationship.*

7. SIMULATION OF ROCK CUTTING

The rock sample 109 × 109 mm representing sandstone with properties determined in the previous section will be used as the rock sample in cutting simulation. Geometry of the analysed problem of rock cutting is shown in figure 7a. The cutter is treated as rigid, the rake angle is 30°, and the cutting depth is 30 mm. The interaction between the tool and rock is modelled assuming the stiffness in the normal and tangential direction $k_n^{rt} = k_T^{rt} = = 20$ GPa and the Coulomb friction coefficient $\mu^{rt} = 0.3$. Cutting velocity was assumed 4 m/s. The failure mode of rock during cutting is shown in figure 8. It can be seen that a typical failure for brittle rocks is reproduced.

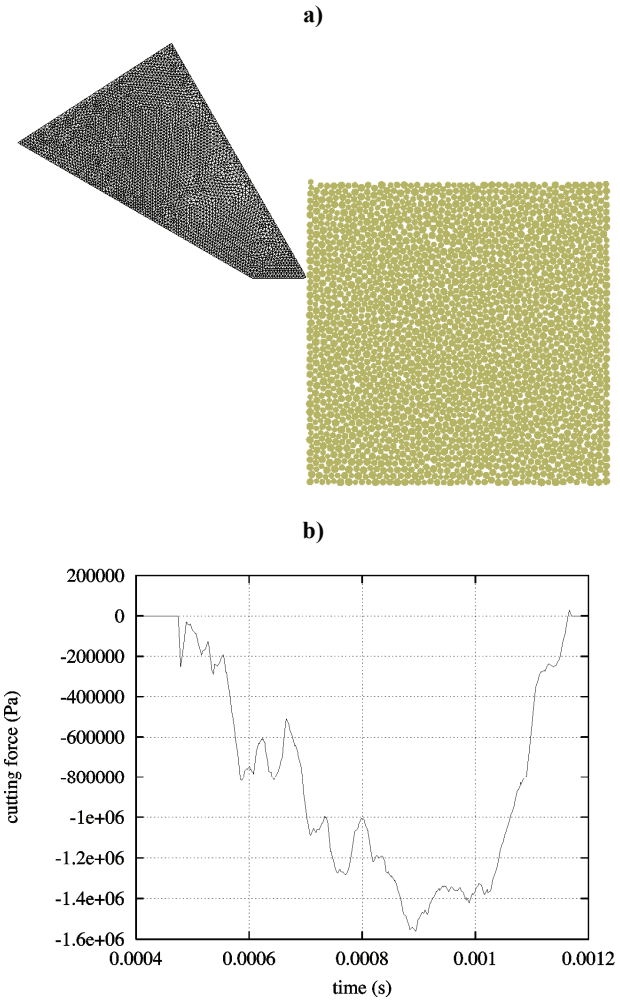

Fig. 7. Simulation of rock cutting: a) discrete element model of rock cutting, b) variation of cutting force.

Variation of the total cutting force is shown in figure 7b. For given rock properties (σ_t = 12.7 MPa) and cutting process parameters (cutting depth d = 0.03 m and rake angle α = 30°) formula (1) yields the cutting force predicted by the Evans' model

$$F_c = \frac{2 \cdot 12.7 \cdot 10^6 \cdot 0.03 \cdot 1 \cdot \sin 30^\circ}{1 - \sin 30^\circ} \text{N} = 0.762 \cdot 10^6 \text{N},$$

In the numerical curve for the cutting force (figure 7b) we can observe several peaks corresponding to splitting subsequent chips as can be seen in figure 8. The value of the theoretical cutting force $0.762 \cdot 10^6$ N agrees quite well with the peak value, $0.8 \cdot 10^6$ N, corresponding to the splitting of the second chip (at time instant t = 0.0065 s).

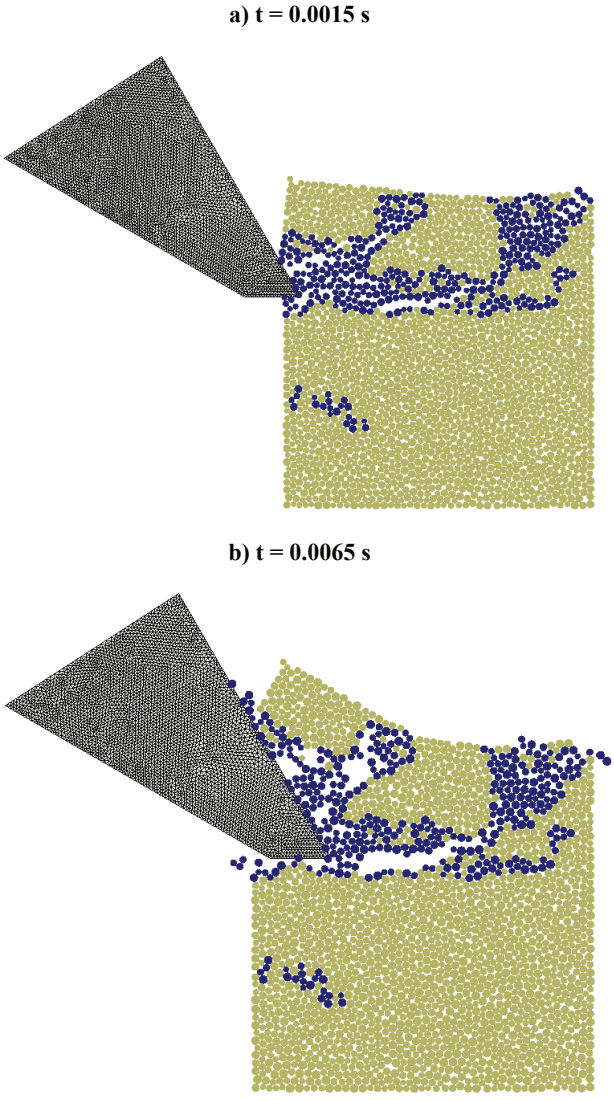

Fig. 8. Failure mode during rock cutting.

In order to predict the cutting force according to Nishimatsu model, the shear strength τ_u and internal friction angle ϕ will be determined first from approximate formulae

$$\tau_u = \frac{\sigma_t \sigma_c}{2\sqrt{\sigma_t(\sigma_c - 3\sigma_t)}} = \frac{12.7 \cdot 60}{2\sqrt{12.7(60 - 3 \cdot 12.7)}} \text{MPa} = 22.8\text{MPa},$$

$$\phi = \arctan\frac{\sigma_c^2 - \sigma_t^2}{4\sigma_c \sigma_t} = \arctan\frac{60^2 - 12.7^2}{4\sigma_c \sigma_t}\frac{12.7 \cdot 60}{4 \cdot 60 \cdot 12.7} = 16^{\circ}.$$

Introducing these values into equation (2) we obtain the cutting force according to the Nishimatsu model

$$F = \frac{2 \cdot 22.8 \cdot 10^6 \cdot 0.03 \cdot 1 \cdot \cos 16^{\circ}}{(1+1)(1 - \sin(17^{\circ} + 16^{\circ} - 30^{\circ}))}\text{N} = 0.69 \cdot 10^6 \text{ N},$$

which is in a pretty good agreement with the numerical values corresponding to initial chip splitting.

8. CONCLUSIONS

Numerical simulation of rock cutting using the discrete element method has given quite satisfactory results in 2D simulation. Further validation is planned carrying out 3D simulation and using laboratory cutting test for comparison.

REFERENCES

Cundall, P.A., 1988, Formulation of a Three Dimensional Distinct Element Model – Part I. A Scheme to Detect and Represent Contacts in a System of Many Polyhedral Blocks, *Int. J. Rock Mech., Min. Sci. & Geomech. Abstr.*, 25(3), 107–116.

Cundall, P.A., Strack, O.D.L., 1979, A discrete numerical method for granular assemblies, *Geotechnique*, 29, 47–65.

Evans, I., 1965, The force required for pointed attack picks, *Int. J. Min. Engng.*, 2, 63–71.

Huang, H., 1999, *Discrete Element Modeling of Tool-Rock Interaction*, PhD thesis, University of Minnesota.

Nishimatsu, Y., 1972, The mechanics of rock cutting, *Int. J. Rock Mech. Mining Sci.*, 9, 261–270.

Podgórski, J., Jonak, J., 2004, *Numeryczne badania procesu skrawania skał izotropowych*, Lubelskie Towarzystwo Naukowe, Lublin (in Polish).

Rojek, J., Oñate, E., Zarate, F., Miquel, J., 2001, Modelling of rock, soil and granular materials using spherical elements, *2nd European Conference on Computational Mechanics ECCM-2001*, Cracow, 26-29 June, 2001.

Williams, J.R., O'Connor, R., 1999, Discrete Element Simulation and the Contact Problem, *Archives Comp. Meth. Engng*, 6(4), 279–304.

MODELOWANIE SKRAWANIA SKAŁ METODĄ ELEMENTÓW DYSKRETNYCH

Streszczenie

Artykuł prezentuje numeryczne modelowanie procesów skrawania skał metodą elementów dyskretnych. W modelowaniu zastosowano metodę elementów dyskretnych wykorzystującą sztywne elementy cylindryczne i sferyczne. Algorytm numeryczny został implementowany we własnym programie komputerowym autora. Metoda elementów dyskretnych jest powszechnie uznaną za doskonale nadającą się do modelowania zagadnień z nieciągłościam występujących w mechanice skał. Możliwości metody w modelowaniu zniszczenia skał pokazano w kilku przykładach numerycznych. Przykłady numeryczne obejmują symulacje prób wytrzymałościowych oraz skrawania skały. W symulacji uzyskano realistyczną postać zniszczenia skały. Poprawność wyników numerycznych oceniono przez porównanie z przewidywaniami teoretycznymi.

Submitted: September 20, 2006
Submitted in a revised form: December 5, 2006
Accepted: December 5, 2006